HOKKAIDO UNIVERSITY

Title	High-temperature carburization behaviour of HASTELLOY X in CH4 gas
Author(s)	Matsukawa, Chihiro; Hayashi, Shigenari; Yakuwa, Hiroshi et al.
Citation	Corrosion Science, 53(10), 3131-3138 https://doi.org/10.1016/j.corsci.2011.05.056
Issue Date	2011-10
Doc URL	https://hdl.handle.net/2115/47204
Type	journal article
File Information	CS53-10_3131-3138.pdf

Hokkaido University Collection of Scholarly and Academic Papers : HUSCAP

High-temperature Carburization behaviour of HASTELLOY X in CH_4 gas

Chihiro Matsukawa[a], Shigenari Hayashi[a], Hiroshi Yakuwa[b], Tadahiko Kishikawa[b], Toshio Narita[a], Shigeharu Ukai[a]

[a]Faculty of Engineering, Hokkaido University, Sapporo, Japan
[b]EBARA Corporation, Japan

Abstract

Ni-base wrought alloy HASTELLOY X* tube was exposed to Ar-CH_4 at 800 and 1000 ˚C in order to understand the carburization kinetics of the alloy used for fuel injection nozzles of micro-gas turbine combustors. Three different internal carbides, $(Cr,Mo)_3C_2$, $(Cr,Mo)_7C_3$ and $(Cr,Mo)_{23}C_6$ were observed in this order from the surface, and the partial damage to the outer surface of the specimen tube appeared similar to metal-dusting. The internal carburization kinetics on both the inner and outer parts of tube followed the parabolic rate law. The carbon permeability in HASTELLOY X was obtained, and was slightly smaller than that of Ni-20%Cr.

Key words

High-temperature corrosion, Carburization, Ni-base alloy, Metal dusting, carbon diffusion

Footnote

*: Hatelloy is the registered trademark of Haynes International, Inc.

1. Introduction

HASTELLOY X is widely used as a high-temperature material for gas-turbine components such as combustors and fuel injection nozzles. This alloy provides excellent oxidation resistance in high temperature oxidizing atmospheres by forming a protective Cr_2O_3 scale [1]. However, this alloy is frequently exposed to low-oxygen potential, high-carbon activity atmospheres, particularly in combustion environments with methane and propane gases, which are widely used. The Cr_2O_3 protective oxide scale is expected to be unstable in such environments and may fail to provide protection. Moreover, these carbonaceous gases are known to cause carburization [2] [3] and, in some cases, metal-dusting [4] [5]. We have observed significant metal loss occurring at the tip section of fuel injection nozzles of HASTELLOY X in micro-gas turbine combustors operated with CH_4 gas.

Carburization studies of Fe and Ni based Cr alloys have been widely reported. For example, Smith *et al.* tested several commercial Fe-Cr-Ni alloys (Fe -19.8~45.7 wt.% Ni -21~35.5 wt.% Cr) in C_3H_6/H_2 atmosphere at 900-1100 ˚C, and reported the formation of partial external Cr_3C_2 scale and internal carbides of $Cr_{23}C_6$ and Cr_7C_3. The internal carburization kinetics of all alloys tested were found to follow parabolic kinetics, and reactive elements such as Nb, Al, Mo and Si reduced the internal carburization rates. They also recognized a dependence of the carburization kinetics on the substrate Ni/Fe ratio, but did not discuss this in depth [6]. The carbon diffusivity is reported to increase with increasing alloy Ni content up to 60 wt.%, and then decreases with further increase in Ni up to 80 wt.% [7] [8]. Therefore it is expected that the alloy Ni/Fe content should have an effect on the internal carburization kinetics. Generally, commercial alloys contain various alloying elements and different Fe and Ni content. This variety in alloy compositions makes it quite difficult to interpret the corrosion behaviour of different alloys, for example HASTELLOY X, in actual operating environments.

However, while the above-mentioned HASTELLOY X alloy is widely used for combustor components, carburization studies on HASTELLOY X are very limited. A study by Muraoka *et al.* using HASTELLOY X was only the specific report we found, however they used solid carbon for their carburization study [9], and there was no information about corrosion by gaseous carbon containing species. In order to understand the corrosion of the alloy used for fuel injection nozzles in micro-gas turbines, we investigated the carburization behaviour of HASTELLOY X in Ar-CH_4 gas mixture at 800 and 1000 ˚C.

2. Experimental procedures

Carburization samples with 20 mm length were cut from a wrought HASTELLOY X tube, with inner and outer diameters of 9.1 and 10.7 mm, respectively. Both the inner and outer surfaces of the tube samples were finished with 1200 grit SiC paper, followed by ultrasonic cleaning in methanol-benzene prior to carburization testing. Plate shape samples with 1.5 mm thick were also used for some corrosion tests in order to identify the products formed on the sample after the corrosion test by X-ray diffraction (XRD). The composition of the HASTELLOY X alloy is shown in Table 1. Figure 1 shows a schematic illustration of the carburization equipment used in this study. The test specimen was set in the furnace hot zone by placing it on top of an alumina tube.

In this setup, the Ar or reaction gases were supplied from the bottom of the alumina tube, through the middle of the tubular specimen, then into the reaction quartz tube. The carburization test was conducted for up to 100 h at 800 or 1000 ˚C. The reaction tube was flushed with Ar gas several times prior to each corrosion test. The furnace temperature was increased at a rate of 10 ˚C / min to the carburization temperature, 800 or 1000 ˚C, with an Ar flowing gas stream, at a flow rate of 200 cm^3 / min. When the carburization temperature was reached the Ar gas was changed to an Ar-10%CH_4 mixture with a flow rate of 150 cm^3 / min. After the carburization test, the specimen was furnace cooled in the carburization gas stream with a flow rate of 50 cm^3 / min.

The inner and outer surfaces and cross-sectional microstructures of the carburized specimens were examined by scanning electron microscopy (SEM) and optical microscopy (OM). Murakami's reagent, which contains 1.78 mol KOH and 0.304 mol $K_3[Fe(CN)_6]$ per litre, was used for etching the cross-sections in order to distinguish between the internal carbide. Some of the specimens were analyzed by electron probe micro-analyzer (EPMA) and XRD to determine the distribution of each element and identify the structures of the reaction products.

3. Results

Surface morphologies

Figure 2 shows the surface morphologies of the specimens after carburization tests at 800 and 1000 ˚C for 1, 4, 25 and 100 h. Scratches from surface grinding can still be observed after 25 h of carburization at 800 ˚C, and the surface was covered with a needle-like reaction product after 100 h. At 1000 ˚C, both the inner and outer surfaces were covered by a fine-grained reaction product after 1 hour of carburization, and the fine-grained product became coarser after longer carburization. On the outer surface, a coarse spherical shaped reaction product was observed after 25 h of carburization and tended to grow larger after 100 h. This spherical reaction product (Fig. 2 (e), (f)) was found to be a thin film and easily peeled from the surface as shown in Figure 3 (a) (Fig. 3 (a) was obtained from a much longer carburization test). This reaction product was identified as graphite from XRD analysis, Figure 3 (c). As shown in Figure 3 (b), a small amount of Ni and Cr_3C_2 particles were observed to form at the bottom of the graphite film. Moreover, Cr_3C_2 scale formation was also confirmed in areas where no-graphite film was formed.

Cross-sectional microstructure

Figures 4 and 5 show cross-sections of the end of the specimen tubes after carburization tests at 800 and 1000 ˚C for different carburization times. At 800 ˚C no internal carburization was observed for at least 25 h of carburization, but was observed in some areas after 100 h in the inner part of the tube. At 1000 ˚C, the internally carburized layers were observed to develop after 1 hour, and the depth of each layer increased with time. The rate of growth of the inner and outer regions carburization zones was different during shorter reaction times. The depth of the inner carburization zone was greater than the outer zone until 4 h of corrosion, but they became almost equal after 9 h. After 25 h of carburization, the internal carburization zone was found to consist of three different layers (Fig. 5 (d)). The outermost layer finally reached the centre of the specimen after 100 h.

Figure 6 shows cross-sectional microstructures of the near-surface region of the specimen tube inner surface before (Fig. 6(f)) and after carburization tests at 1000 ˚C. The alloy substrate before carburizing contains small precipitates, in bright contrast. From our separate study, this primary precipitates were found to be rich in Mo [10] and would be M_6C type carbide [11]. After carburization tests, carbides, in dark

contrast, were found to form and grow mainly along grain boundaries and the interfaces between Mo-rich precipitates and the substrate.

Figure 7 shows the results of EPMA analysis of the carburized specimen after 9 h at 1000 ˚C, and all the carbides were high in Cr and low in Mo. The carbides were identified from their metal/carbon ratio to be M_3C_2, M_7C_3 and $M_{23}C_6$ (M = Cr and Mo) in this order from the surface. Figure 8 shows cross-sectional microstructures of each part of the specimen carburized for 100 h at 1000 ˚C. Apart from the inner middle part of the tube specimen (Fig. 8 (b)), after carburization the surfaces became significantly rough and powder-like metal particles were also observed, particularly at the tip of the tube. Areas that were significantly damaged were found to correspond to the locations where graphite film formation was observed, as shown in Figure 3.

Growth kinetics of the carburization zone

Figure 9 shows the depth of each carbide layer from the surface as a function of the square root of carburization time. During shorter carburization times up to 16 h, the linear correlation indicated that growth followed parabolic kinetics. The reaction front of the $M_{23}C_6$ layer reached the centre of the specimen after about 16 h of carburization, but the M_3C_2 and M_7C_3 layers still continued to grow deeper, and finally the internal carbide was almost completely M_3C_2 after 100 h.

4. Discussion

Carbon activity of the test reaction gas

CH_4 can dissociate into H_2 and C through the following reaction.

$$CH_4 = 2H_2 + C \qquad (1)$$

The temperature dependence of the equilibrium constant K of eq. (1), in Figure 10, shows that carbon activity increases with increasing temperature [12]. The carbon activity, a_c, is expressed in terms of K by using partial pressures of CH_4, P_{CH4}, and H_2, P_{H2}, as:

$$a_c = \frac{P_{CH_4}}{P_{H_2}^{\ 2}} K \qquad (2)$$

and a_c can be calculated by the ratio of partial pressures of CH_4 and H_2. In this study the carbon activity was high enough to cause carburization at both temperatures, however, the initial carbon activity could not be calculated because an Ar-CH_4 gas mixture without H_2 was used, and the extent of CH_4 dissociation was not measured.

Formation and growth of three different carbides

M_3C_2, M_7C_3 and $M_{23}C_6$ were found to form, in this order from the surface, in this study. Among those Cr carbides, $Cr_{23}C_6$ is the most stable carbide, forming in the innermost region. During the initial transient stage, carbon diffuses into the substrate, forming $M_{23}C_6$ carbide in the sub-surface region, followed

by M_7C_3 and M_3C_2 formation with longer reaction time due to increasing carbon activity in the substrate. When graphite nucleated at the alloy surface, a_c at the graphite/alloy boundary became unity. The growth kinetics of each carbide layer then continued in a steady state until carbon reached the centre of substrate, as illustrated in Figure 11. During the steady state growth of each carbide layer, $M_{23}C_6$ and M_7C_3 were carburized to form M_7C_3 and M_3C_2, respectively. After the $M_{23}C_6$ layer reached the centre of the specimen, M_7C_3 and M_3C_2 continue to grow deeper until carbon activity in the substrate become uniform, and only M_3C_2 remained.

Although the solubility products of the carbides are relatively large, Wagner's theory [13] can be applied in this study [12]. As the carbon permeability $N_C^{(S)}D_C$ is expected to be much greater than that of Cr [12], the condition can be described as

$$N_C^{(S)} D_C >> N_{Cr}^{(0)} D_{Cr} \qquad (3)$$

Here, $N_C^{(S)}$ and $N_{Cr}^{(0)}$ are mole fractions, and D_C and D_{Cr} are diffusion coefficients of solute carbon and Cr, respectively. The depth of the carburized zone X is expressed by Eq. (4) as a function of corrosion time, t, when the growth of the internal carburization zone is diffusion controlled.

$$X^2 = 2k_p t \qquad (4)$$

When Eq. (3) is satisfied, the parabolic rate constant k_p is described by Eq. (5) [12],

$$k_p = \frac{\varepsilon N_C^{(s)} D_C}{\nu N_M^{(o)}} \qquad (5)$$

where $N_M^{(0)}$ is the original alloy concentration of metal M which forms carbide MC_ν and ν is the stoichiometric number of carbide (C per one atom of M). ε is the diffusion blocking parameter by the internal precipitates.

For up to 9 h of carburization, where the carburized layer had not reached the centre of the specimen, the k_p of $M_{23}C_6$ was obtained from Figure 9 by using Eq. (4) to be $k_p = 2.9 \times 10^{-8}$ [cm^2 sec^{-1}] for the inner surface and $k_p = 3.6 \times 10^{-8}$ [cm^2 sec^{-1}] for the outer surface of the tube as shown in Figure 12.

The permeability of carbon in HASTELLOY X can be calculated by Eq. (5) using those parabolic rate constants, k_p, and initial alloy Cr content, N_{Cr} =0.244, with the assumption that the blocking factor is negligible, ε = 1. The average of stoichiometric factor [14] of each carbide, ν = 0.452, was used in this study to simplify the calculation, since the widths of carbides zones are similar. The calculated permeabilities of carbon at the inner and outer part of the tube were $N_C^{(S)}D_C = 32 \times 10^{-10}$ [cm^2 sec^{-1}] and 40×10^{-10} [cm^2 sec^{-1}], respectively. Although the obtained permeabilities in this study are slightly smaller than that of Ni-20Cr, $N_C^{(S)}D_C = 55 \times 10^{-10}$ [3], the growth of carbides in HASTELLOY X can be approximated by carbon diffusion in a simple binary Ni-Cr alloy. The alloying elements of Fe, Mo and Si may reduce the carbon permeability in HASTELLOY X, since those elements are reported to reduce the diffusivity of carbon [7] [8] [12]. Further detailed analysis and measurements of the Cr content in the alloy substrate, and the volume fraction of each carbide are required to obtain the individual growth kinetics for each carbide layer, however the carbides were too small to analyze by EPMA.

The difference in carburization rate between inner and outer surface of the tube

The depth of carburization zone at the inner part of the tube was larger than that of the outer part, particularly during the shorter time carburization as shown in Figure 9. However the rate constant of carburization, k_p, of the inner part was slightly lower than that of the outer part as shown in Figure 12. During heating in flowing Ar, a thin Cr_2O_3 scale may form on the HASTELLOY X substrate, because the impurity oxygen in Ar (99.9995 % pure, $O_2 \leq 0.2$ ppm) is still sufficient to form Cr_2O_3 scale. This initially formed Cr_2O_3 scale may result in an incubation period prior to carburization, and complete gas exchange in the reaction tube from Ar to carburization Ar-CH_4 gas mixture needs some amount of time, ~10min. In the present study, the reaction gas was supplied through the tube specimen placed on the Al_2O_3 tube, causing an initial difference in CH_4 concentration between the inner and outer parts of the sample tube. During the gas change, the inner part of the tube surface is expected to start to have been exposed to Ar-CH_4 earlier than the outer part of the sample surface, resulting in the shorter incubation period for the inner part of the tube surface.

In the present study, we could not measure the temperatures at the inner and outer surface of the HASTELLOY X tube. However, we may assume that the temperatures at the outer and the inner surface of tube were not significantly different, since the sample thickness, 0.8 mm, is expected to be thin enough to maintain the sample temperature uniformly under the present experimental condition. With this assumption, there may be two possibilities, different gas temperature and gas flow rate, which caused different carburization kinetics and graphite deposition behaviour at inner and outer part of sample tube. Lower parabolic rate constant of carburization, k_p, observed in the inner part of tube may suggest a lower carbon activity inside the sample tube, which indicates lower gas temperature. However, further discussion, particularly considering the effect of gas flow rate on the carburization behaviour, is difficult, further investigation is required.

Metal dusting

The outer tube surface was found to be significantly damaged, as shown in Figure 8, and graphite deposition was always found on those damaged areas. Young *et al*. reported that the graphite, which can be precipitated on the surface by reaction (1), can grow and incorporate Ni particles, and those Ni particles catastrophically accelerate the reaction causing metal dusting [12]. As mentioned previously, Ni particles were found below the graphite film in the present study (see Fig. 3 (b)), and therefore metal dusting may also have occurred on the HASTELLOY X alloy in Ar-CH_4 atmosphere at 1000 ˚C, after a relatively long exposure time of 100 h. One of the main causes of severe corrosion of micro gas turbine components made from HASTELLOY X alloy may be metal dusting.

6. Conclusions

Carburization of HASTELLOY X alloy at 800 ˚C and 1000 ˚C in Ar-10%CH_4 gas was conducted. The results may be summarized as follows.

1. Internal carburization occurred both at 800 ˚C and 1000 ˚C in Ar-10%CH_4. Much longer incubation periods were observed at 800˚C. Three layered internal carburization zones with M_3C_2, M_7C_3 and $M_{23}C_6$ (M = Cr and Mo) were formed in this order from the surface.
2. The growth of the internal carburization zones formed on both the inner and outer part of tube followed parabolic kinetics. The permeability of carbon in HASTELLOY X was slightly smaller than that of Ni-20Cr alloy.
3. Metal dusting was observed beneath graphite deposition, and may be one of the causes of severe corrosion of micro gas turbine components.

Acknowledgement

This research was supported by the Grant for Practical Application of University R&D Results under the Matching Fund Method.

References

[1] Y. Saito, T. Atake, T. Maruyama, High Temperature Corrosion of Metals, JME, UCHIDA ROKAKUHO, Tokyo, 1986. pp. 101-109.

[2] A. Shnaas and H. J. Grabke, High-temperature corrosion and creep of Ni-Cr-Fe alloys in carburizing and oxidizing environments, Oxidation of Metals 12 (1978) 387-404.

[3] A. T. Allen and D. L. Douglass, Internal-Carburizing Behavior of Ni-V, Ni-Cr, and Ni-3Nb Alloys, Oxidation of Metals 51 (1999) 199-219.

[4] Y. Nishiyama, N. Otsuka and T. Kudo, Metal dusting behaviour of Cr–Ni steels and Ni-base alloys in a simulated syngas mixture, Corrosion Science 48 (2006) 2064-2083.

[5] Y. Nishiyama, Metal Dusting of Steels and Alloys in Carbon-bearing Gases, Zairyo-to-Kankyo 56 (2007) 84-90.

[6] G. M. Smith, D. J. Young, and D. L. Trimm, Carburization kinetics of heat-resistant steels, Oxidation of Metals 18 (1982) 229-243.

[7] S. K. Bose and H. J. Grabke, Diffusion coefficient of carbon in Fe-Ni austenite in the temperature range 950-1100 °C, Zeitschrift für Metallkunde 69 (1978) 8-15.

[8] T. Wada, H. Wada, J. F. Elliot and J. Chipman, Thermodynamics of the Fcc Fe−Ni−C and Ni−C alloys, Metallurgical and Materials Transactions B 2 (1971) 2199-2208.

[9] S. Muraoka, H. Itami and S. Nomura, Carburization of Hastelloy alloy X, Journal of Nuclear Materials 58 (1975) 18-24.

[10] S. Ford and S. Hayashi, unpublished research.

[11] G. Y. Lai, An investigation of the thermal stability of a commercial Ni-Cr-Fe-Mo alloy, Metallurgical and Materials Transactions A 9 (1978) 827-833.

[12] D. J. Young, High Temperature Oxidation and Corrosion of Metals, Elsevier, Oxford, UK, 2008 pp. 397-453.

[13] C. Wagner, Reaktionstypen bei der Oxidation von Legierungen, Zeitshrift für Elektrochemie 63 (1959) 772-782.

[14] S. Ford, Carburisation and Nitridation of Heat Resisting Steels, PhD Thesis, University of New South Wales, 2005 pp. 161.

Captions

Table 1. Chemical Composition of HASTELLOY X

Fig. 1. Schematic illustration of carburization testing equipment used in this study

Fig. 2. Inner and outer surface morphologies of specimens after carburization at 800 ˚C and 1000 ˚C in Ar-10%CH_4

Fig. 3. (a) Overall image, (b) microstructures and (c) XRD pattern of surface products after 196 h carburization at 1000 ˚C in Ar-10%CH_4

Fig. 4. Optical microscope images of etched specimens after carburization at 800 ˚C in Ar-10%CH_4

Fig. 5. Optical microscope images of etched specimens after carburization at 1000 ˚C in Ar-10%CH_4

Fig. 6. Cross-sectional microstructures of inner surface of specimens after (a) 1 h, (b) 4 h, (c) 9 h, (d) 25 h, (e) 100 h, (f) before carburization test at 1000 ˚C in Ar-10%CH_4

Fig. 7. Cross-sectional microstructure and concentration profile of each carbide region

Fig. 8. Cross-sectional microstructures of the specimen after 100 h carburization at 1000 ˚C in Ar-10%CH_4

Fig. 9. Precipitation depth of (a) inner and (b) outer boundaries of each carbide layer after 100 h carburization at 1000 ˚C and schematic of definition of depth

Fig. 10. Equilibrium constant for gas phase carbon producing reaction (1), standard state is 1 atm [12]

Fig. 11. Schematic of development of carbide precipitation zones

Fig. 12. Parabolic plot of precipitation zone widths after carburization of HASTELLOY X at 1000 ˚C in Ar-10%CH_4

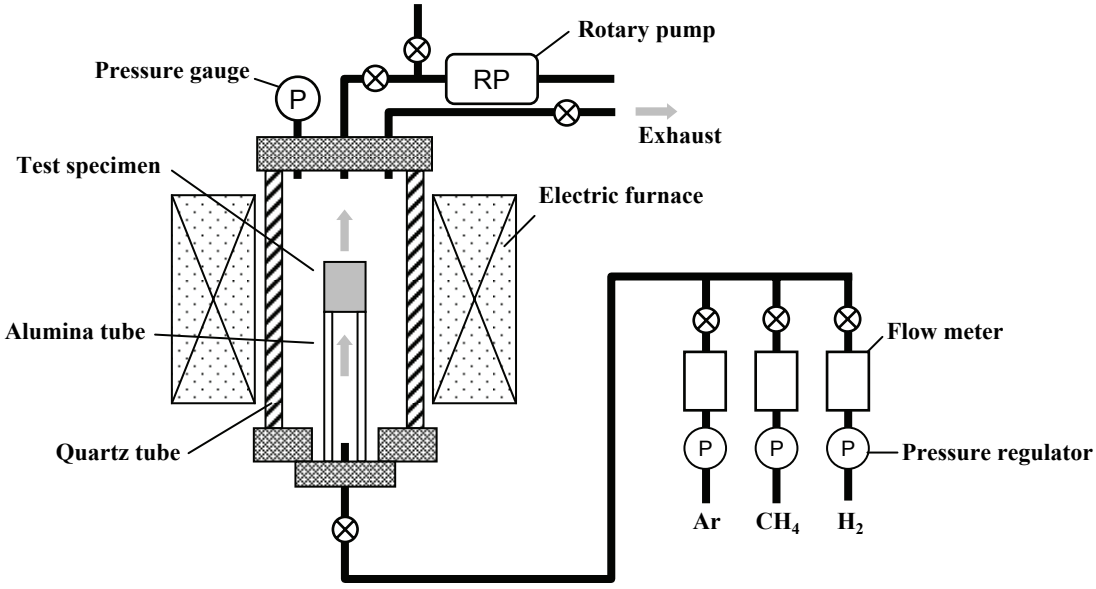
Rotary pump
RP
Pressure gauge
P
Exhaust
Test specimen
Electric furnace
Alumina tube
Flow meter
Quartz tube
P
P
P
Pressure regulator
Ar
CH_4
H_2

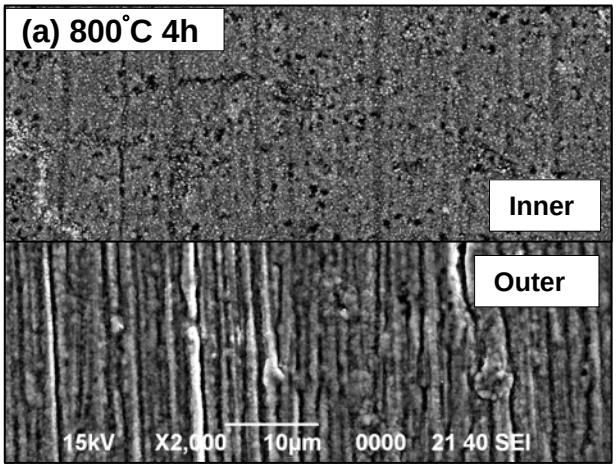
(a) 800˚C 4h
Inner
Outer
15kV X2,000 10μm 0000 21 40 SEI

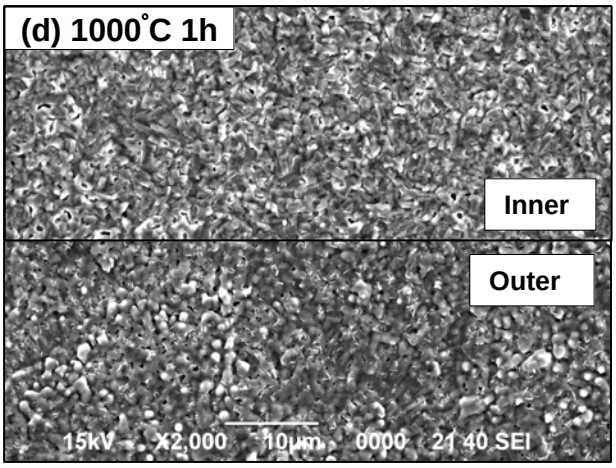
(d) 1000˚C 1h
Inner
Outer
15kV X2,000 10μm 0000 21 40 SEI

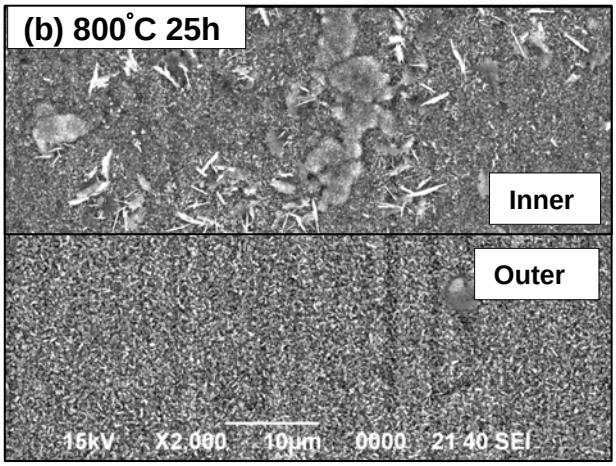
(b) 800˚C 25h
Inner
Outer
15kV X2,000 10μm 0000 21 40 SEI

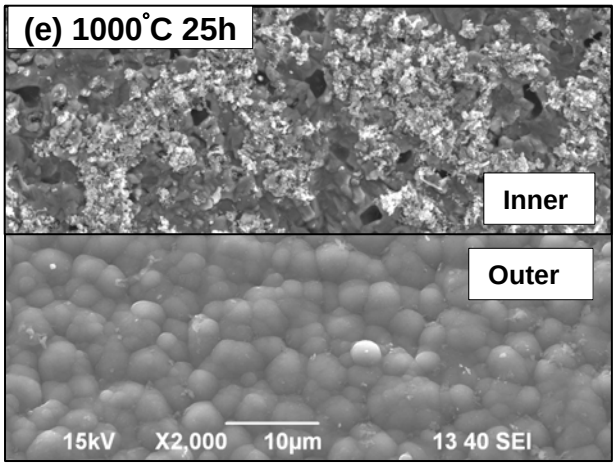
(e) 1000˚C 25h
Inner
Outer
15kV X2,000 10μm 13 40 SEI

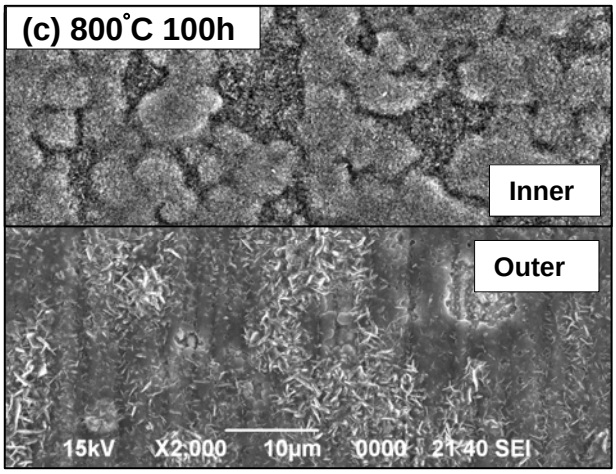
(c) 800˚C 100h
Inner
Outer
15kV X2,000 10μm 0000 21 40 SEI

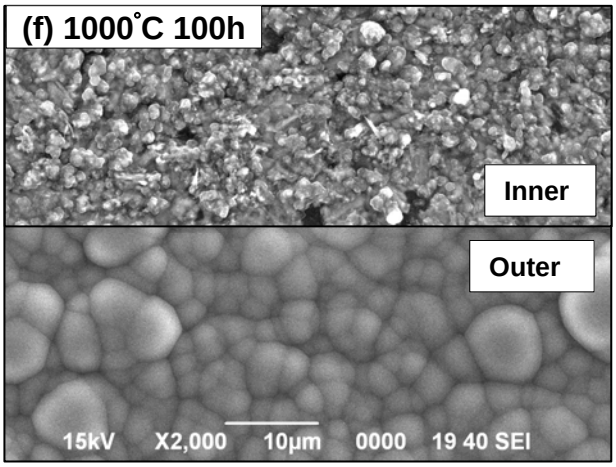
(f) 1000˚C 100h
Inner
Outer
15kV X2,000 10μm 0000 19 40 SEI

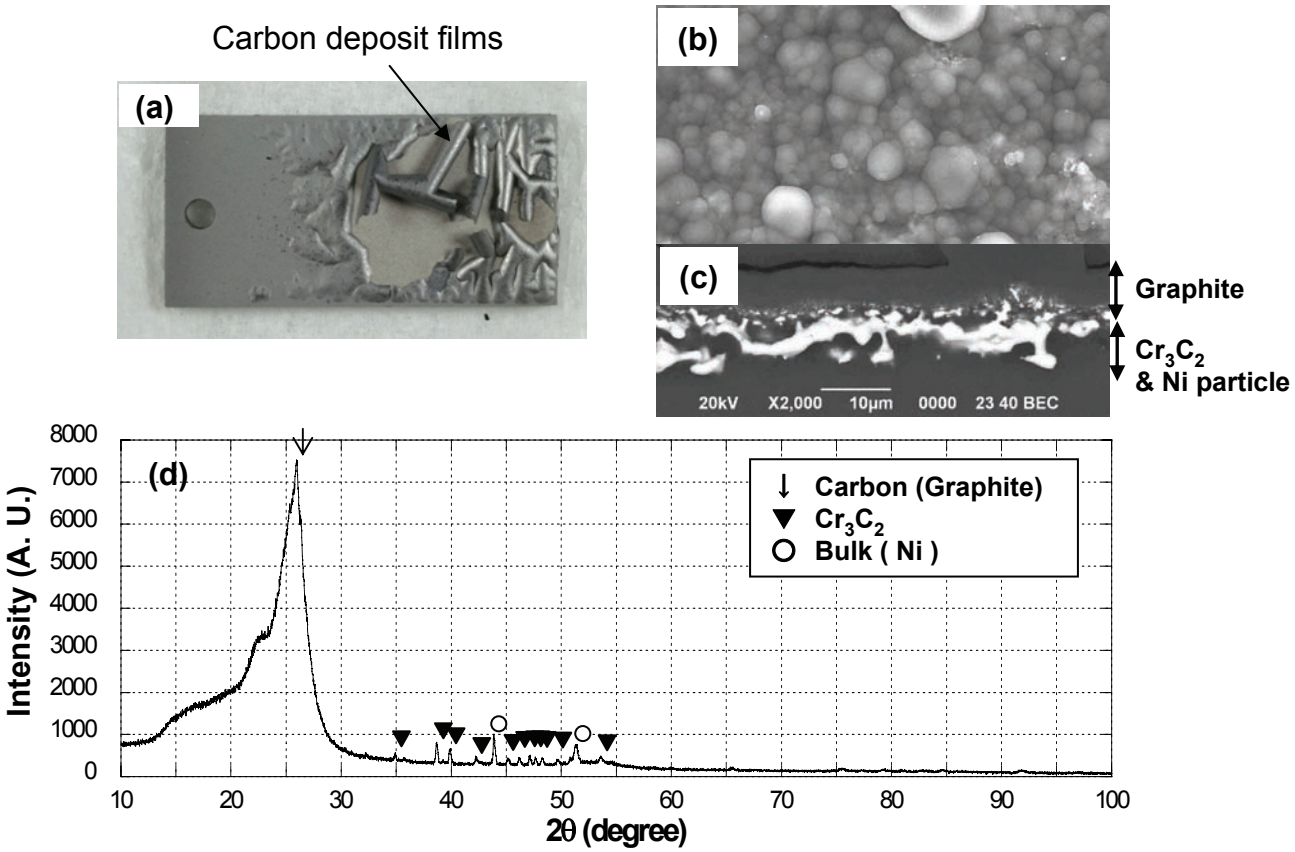
Carbon deposit films
(a)
(b)
(c)
Graphite
Cr_3C_2
& Ni particle
20kV X2,000 10μm 0000 23 40 BEC
(d)
Intensity (A. U.)
2θ (degree)
Carbon (Graphite)
Cr_3C_2
Bulk (Ni)

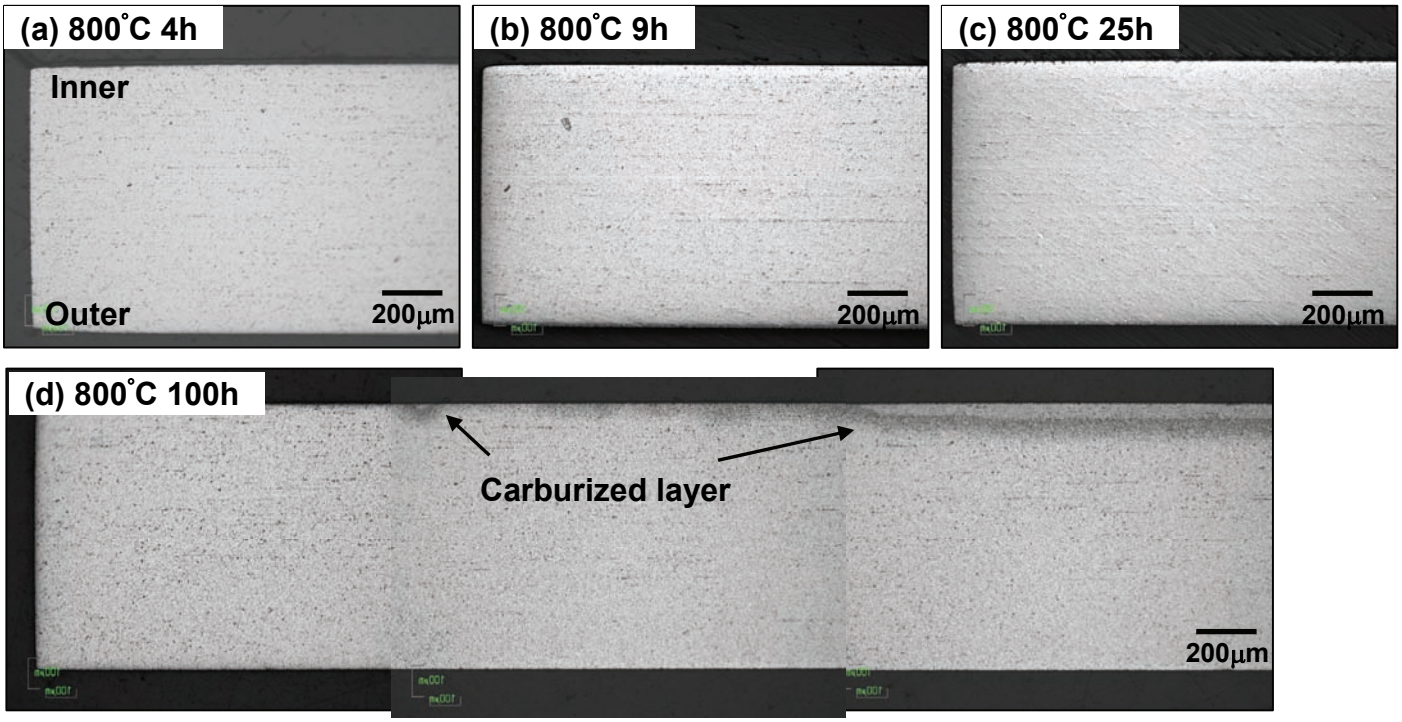
(a) 800˚C 4h
Inner
Outer
200μm
(b) 800˚C 9h
200μm
(c) 800˚C 25h
200μm
(d) 800˚C 100h
Carburized layer
200μm

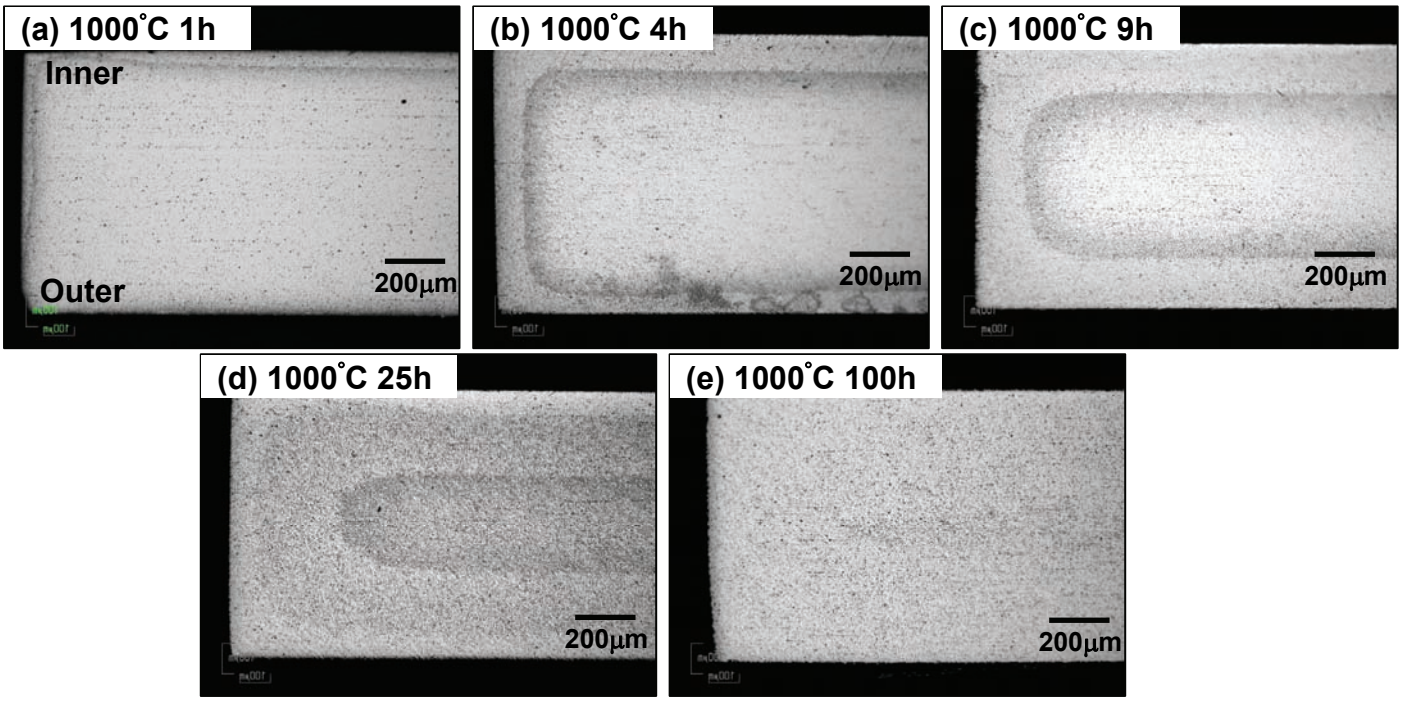
(a) 1000˚C 1h
Inner
Outer
200μm
(b) 1000˚C 4h
200μm
(c) 1000˚C 9h
200μm
(d) 1000˚C 25h
200μm
(e) 1000˚C 100h
200μm

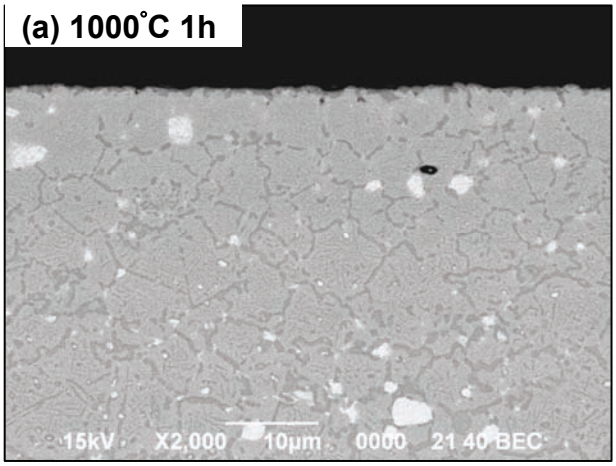
(a) 1000˚C 1h
15kV X2,000 10μm 0000 21 40 BEC

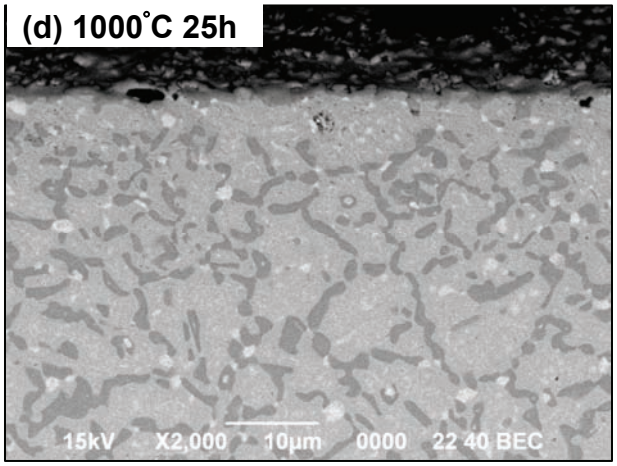
(d) 1000˚C 25h
15kV X2,000 10μm 0000 22 40 BEC

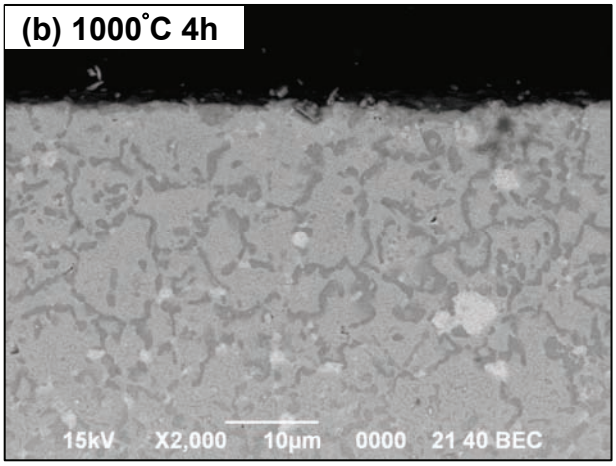
(b) 1000˚C 4h
15kV X2,000 10μm 0000 21 40 BEC

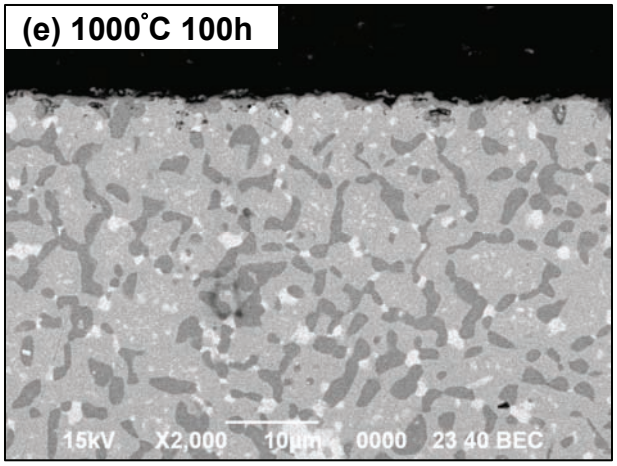
(e) 1000˚C 100h
15kV X2,000 10μm 0000 23 40 BEC

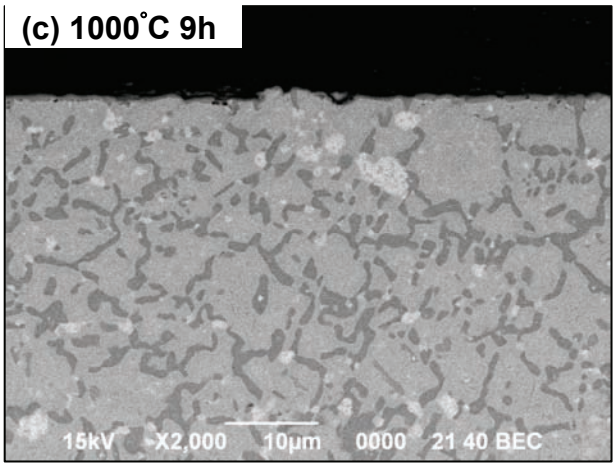
(c) 1000˚C 9h
15kV X2,000 10μm 0000 21 40 BEC

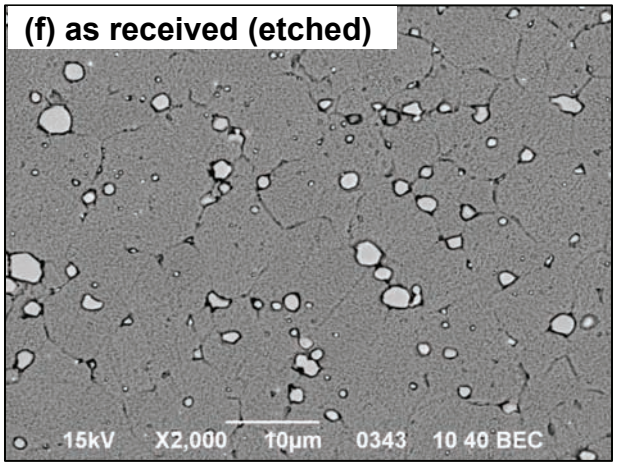
(f) as received (etched)
15kV X2,000 10μm 0343 10 40 BEC

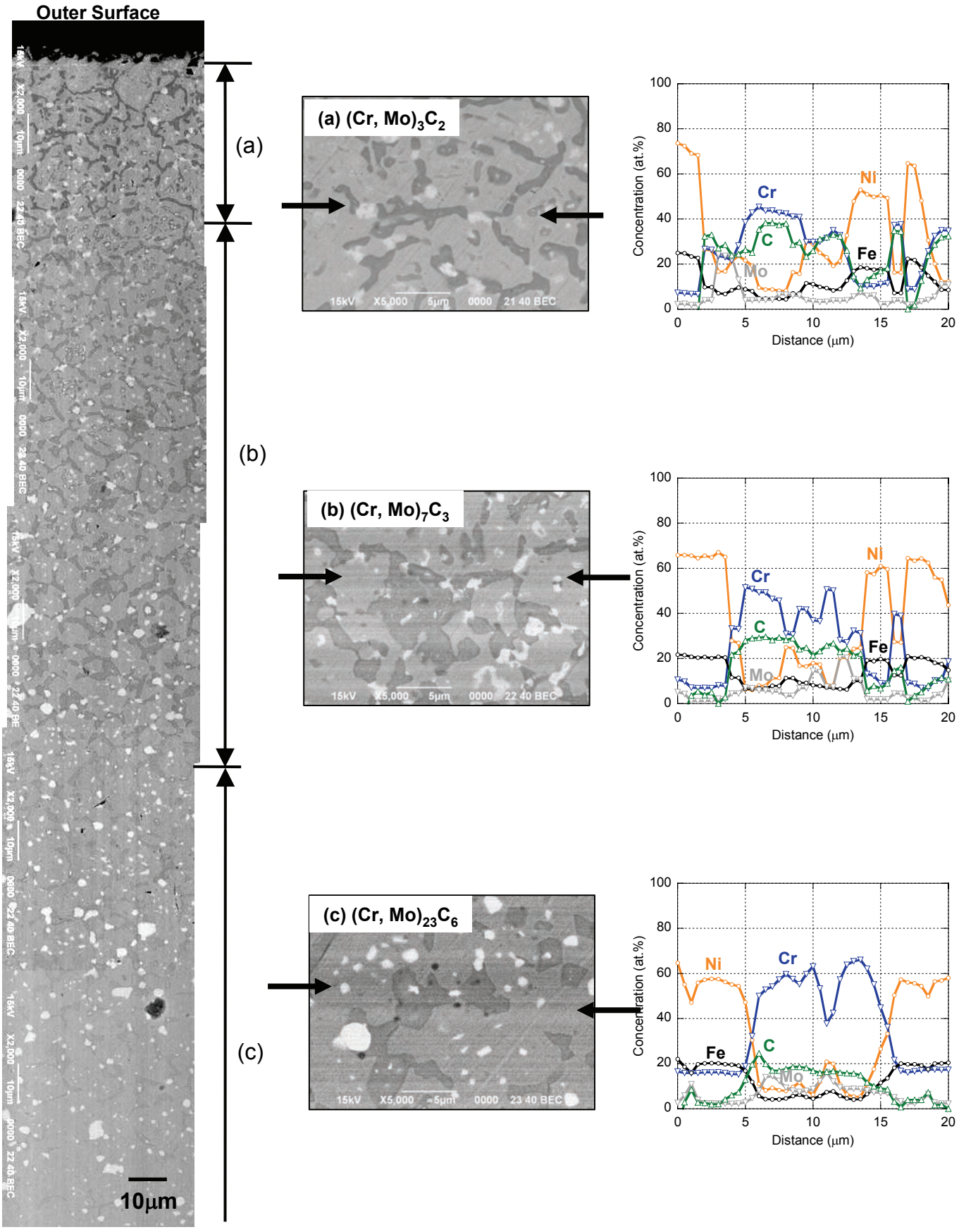
Outer Surface
(a)
(b)
(c)
10μm
(a) (Cr, Mo)3C2
(b) (Cr, Mo)7C3
(c) (Cr, Mo)23C6
Concentration (at.%)
Distance (μm)
Ni
Cr
C
Fe
Mo

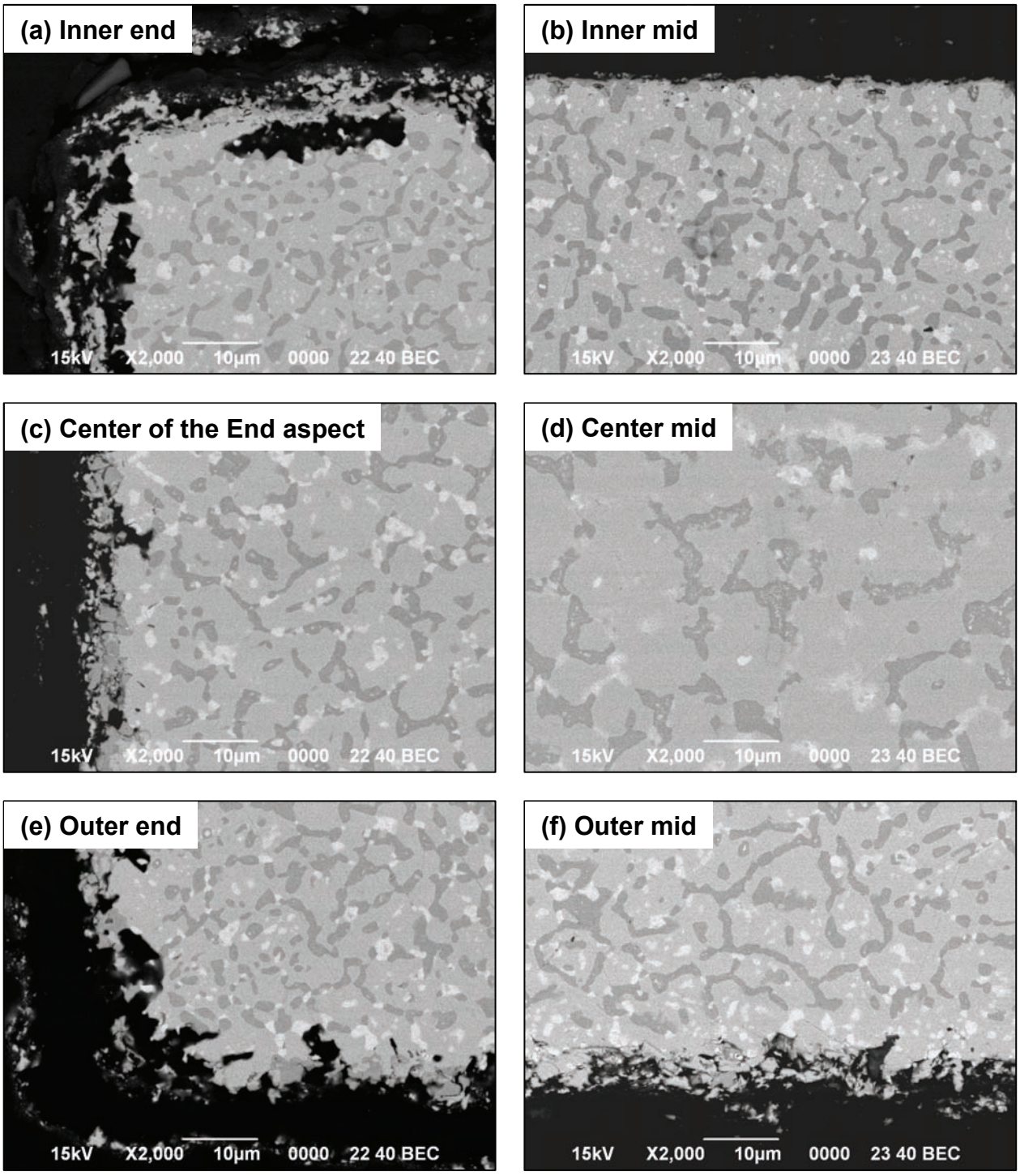
(a) Inner end
15kV X2,000 10μm 0000 22 40 BEC
(b) Inner mid
15kV X2,000 10μm 0000 23 40 BEC
(c) Center of the End aspect
15kV X2,000 10μm 0000 22 40 BEC
(d) Center mid
15kV X2,000 10μm 0000 23 40 BEC
(e) Outer end
15kV X2,000 10μm 0000 22 40 BEC
(f) Outer mid
15kV X2,000 10μm 0000 23 40 BEC

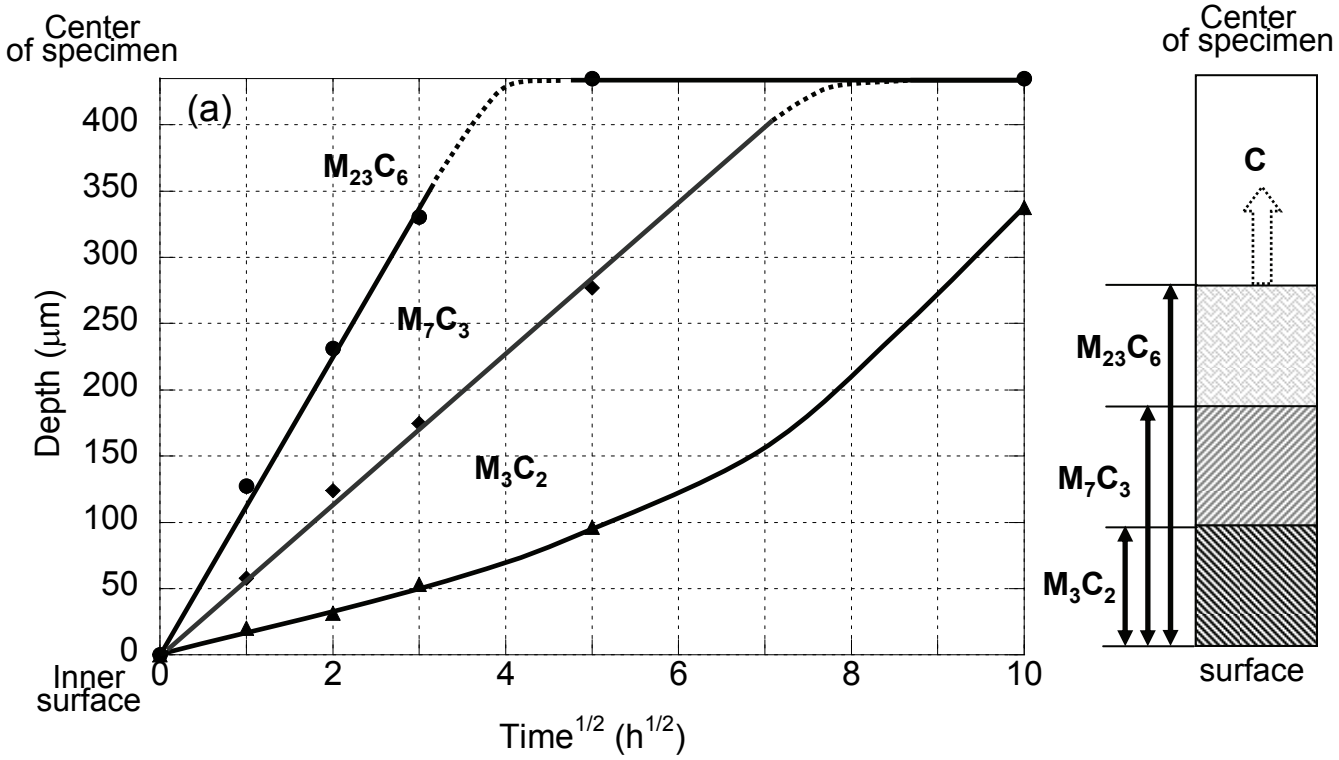
Center
of specimen
(a)
$M_{23}C_6$
M_7C_3
M_3C_2
Depth (μm)
Inner
surface
Time$^{1/2}$ (h$^{1/2}$)
Center
of specimen
C
$M_{23}C_6$
M_7C_3
M_3C_2
surface

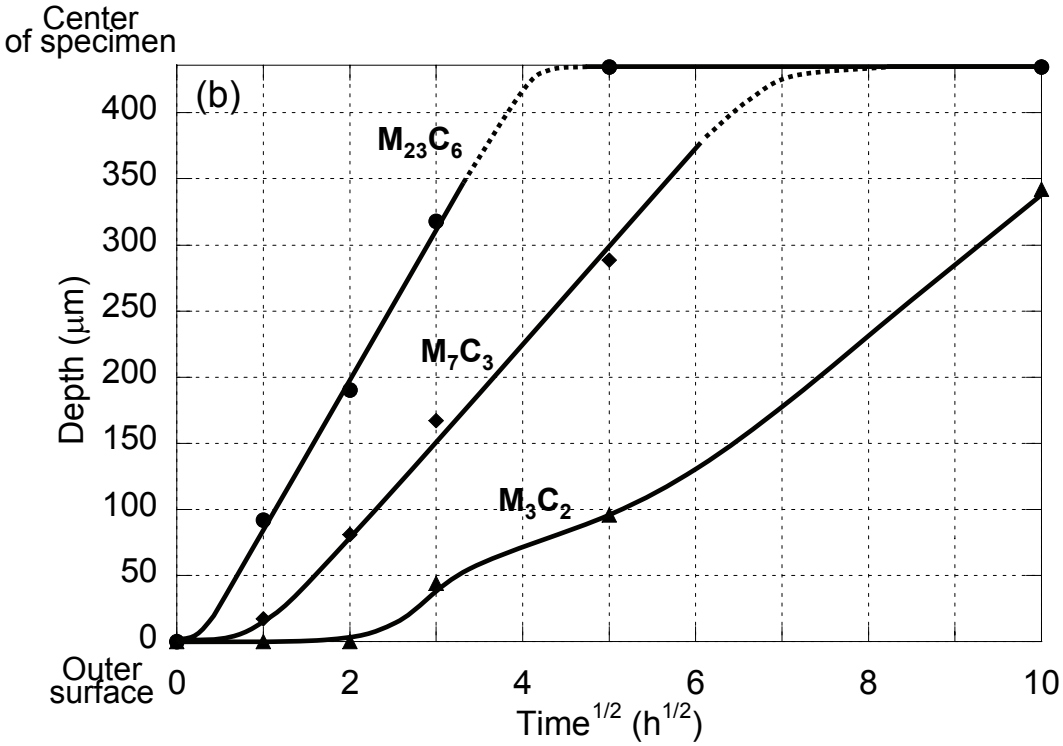
Center
of specimen
(b)
$M_{23}C_6$
M_7C_3
M_3C_2
Depth (μm)
Outer
surface
Time$^{1/2}$ (h$^{1/2}$)

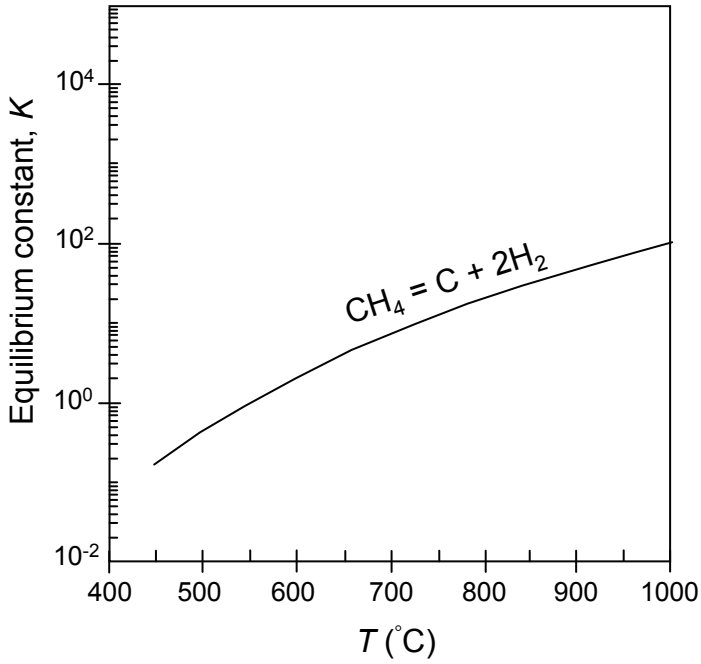
Equilibrium constant, K
10^4
10^2
10^0
10^-2
400
500
600
700
800
900
1000
T (°C)
CH4 = C + 2H2

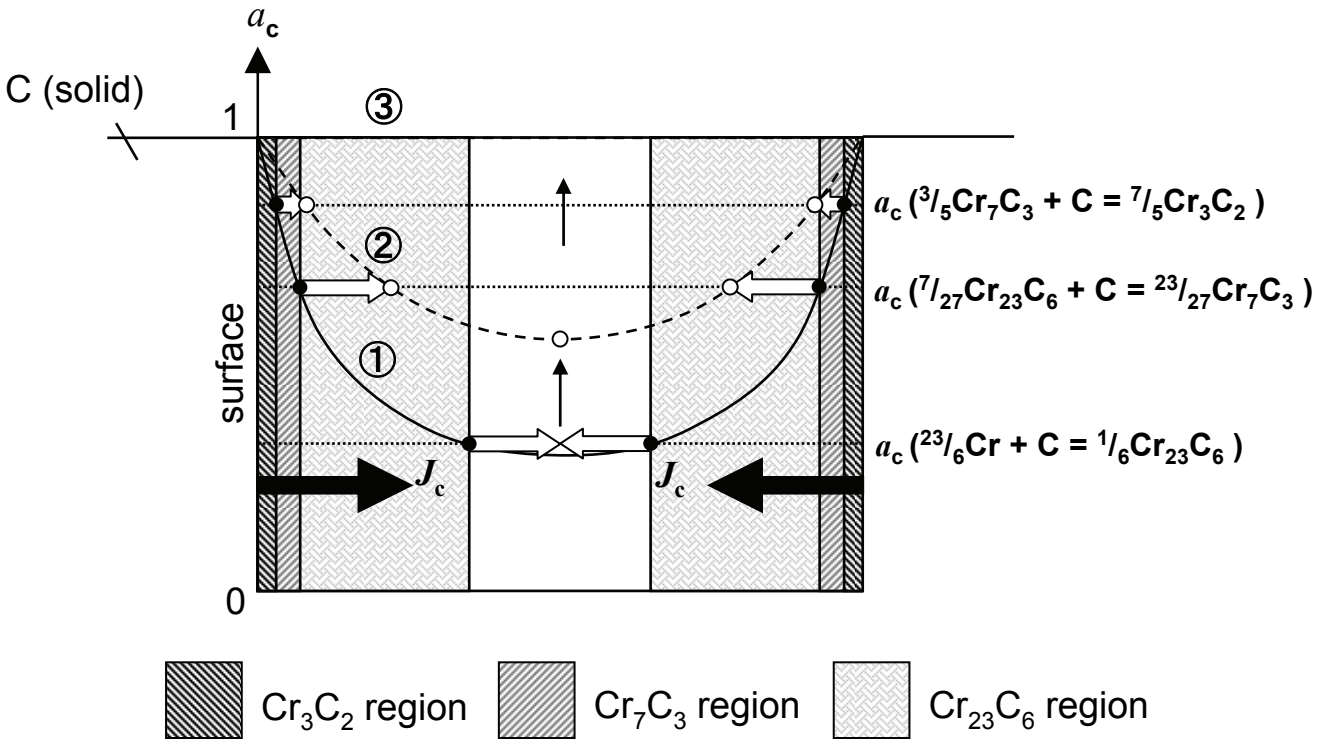
a_c
C (solid)
1
③
②
①
surface
0
a_c ($^3/_5Cr_7C_3$ + C = $^7/_5Cr_3C_2$)
a_c ($^7/_{27}Cr_{23}C_6$ + C = $^{23}/_{27}Cr_7C_3$)
a_c ($^{23}/_6Cr$ + C = $^1/_6Cr_{23}C_6$)
J_c
J_c
Cr_3C_2 region
Cr_7C_3 region
$Cr_{23}C_6$ region

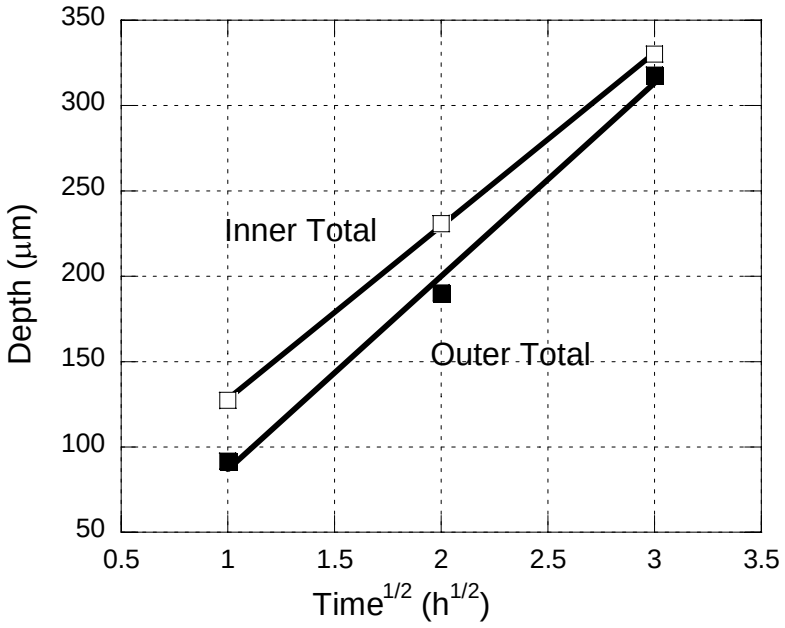
350
300
250
200
150
100
50
Depth (μm)
Inner Total
Outer Total
0.5
1
1.5
2
2.5
3
3.5
Time1/2 (h1/2)

(in wt.%)

Ni	Cr	Fe	Mo	Co	W	C	Mn	Si	B
bal.	22	18	9	1.5	0.6	0.1	1*	1*	0.008

*Maximum